


Instabilities in the yellow hypergiant domain

Wolfgang Glatzel¹★ and Michaela Kraus² 

¹*Institut für Astrophysik (IAG), Georg-August-Universität Göttingen, Friedrich-Hund-Platz 1, D-37077 Göttingen, Germany*

²*Astronomical Institute, Czech Academy of Sciences, Fričova 298, CZ-25165 Ondřejov, Czech Republic*

Accepted 2024 March 20. Received 2024 March 19; in original form 2023 November 2

ABSTRACT

Yellow hypergiants (YHGs) are massive stars that are commonly interpreted to be in a post-red supergiant evolutionary state. These objects can undergo outbursts on time-scales of decades, which are suspected to be due to instabilities in the envelope. To test this conjecture, the stability of envelope models for YHGs with respect to infinitesimal, radial perturbations is investigated. Violent strange mode instabilities with growth rates in the dynamical regime are identified if the luminosity-to-mass ratio exceeds $\approx 10^4$ in solar units. For the observed parameters of YHGs, we thus predict instability. The strange mode instabilities persist over the entire range of effective temperatures from red to blue supergiants. Due to short thermal time-scales and dominant radiation pressure in the envelopes of YHGs, a non-adiabatic stability analysis is mandatory and an adiabatic analysis being the basis of the common perception is irrelevant. Contrary to the prevailing opinion, the models considered here do not exhibit any adiabatic instability.

Key words: instabilities – stars: atmospheres – stars: massive – stars: oscillations – supergiants.

1 INTRODUCTION

The upper domain of the Hertzsprung–Russell (HR) diagram is populated by massive stars ($> 8 M_{\odot}$) in their diverse evolutionary states. One of these stages comprises the yellow hypergiants (YHGs). These stars spread in temperature from about 4000 to 8000 K and have luminosities in the range $5.4 \leq \log L/L_{\odot} \leq 5.8$. YHGs are commonly interpreted as being in their blueward evolution after having passed through a previous red supergiant (RSG) phase (e.g. de Jager 1998; Gordon & Humphreys 2019). According to stellar evolutionary tracks for rotating single stars (e.g. by Ekström et al. 2012), they might have evolved from progenitors with initial masses of 20–40 M_{\odot} because stars in this mass range are suggested to evolve back to the blue, hot side of the HR diagram where they may evolve into hot supergiants, such as the luminous blue variables, B[e] supergiants, or Wolf–Rayet stars. This prediction of the evolutionary models is consistent with the observational finding of an apparent absence of Type II-P supernovae for stars that are initially more massive than $\sim 20 M_{\odot}$ and whose progenitors are RSGs (Smartt 2009). These evolutionary models also predict that stars more massive than 40 M_{\odot} apparently do not evolve into cool RSGs. These stars seem to reach their turning point at significantly higher temperatures from where they evolve back to the blue side, and they do so the earlier (i.e. the hotter) the more massive they are. Consequently, evolution into a YHG is restricted to stars within a very narrow initial mass range, consistent with the position of currently confirmed YHGs in the HR diagram (e.g. Kourniotis et al. 2022).

The distinction between pre- and post-RSG stars in the yellow domain is based on the significant spectroscopic and photometric

variability of the latter. YHGs can also display indication for large-scale nebulae formed from the extensive mass-loss during the RSG phase. This is particularly true for the more massive objects, which transit much faster from the red to the yellow domain, leaving not much time for the released mass to expand and dilute. Indeed, the more massive stars in the currently known sample of Galactic YHGs display either an extended nebulosity (e.g. IRC+10420; Tiffany et al. 2010) or indication for large spherical shells of expanding cold molecular gas (e.g. IRC+10420 and HD 179821; Oudmaijer et al. 2009).

Besides these large-scale ejecta, YHGs can also be embedded in material that the stars have released more recently, most likely during one or more outburst events. Clear indication for such recent ejection episodes has been found for only a few cases, such as the Galactic object IRAS 17163–3907 (also known as the Fried Egg nebula; Lagadec et al. 2011), which seems to have experienced at least three outbursts within the past 100 yr. These outbursts have led to the formation of three individual dust shells around the star (Koumpia et al. 2020).

However, not every outburst releases enough mass to guarantee the production of significant amounts of detectable dust. The prime example is the Galactic object ρ Cas that has experienced at least four outbursts during the past ~ 90 yr (Maravelias & Kraus 2022), but only after its outburst in 1946–1947 emission from dust could be detected that must have formed from the released matter (Jura & Kleinmann 1990). Since then, this dust shell expanded and cooled, but no new dust has formed in detectable amounts from the more recent events (Shenoy et al. 2016).

Ejected circumstellar material can also be traced by static nebular line emission of low-excitation metal lines, such as Fe I, Sr II, Y II, and Ba II (e.g. Lobel et al. 1998; Kourniotis et al. 2022), by emission of forbidden lines such as [Ca II] and [O I], whereby [O I] is typically

* E-mail: wglatze@astro.physik.uni-goettingen.de

seen in hotter YHGs such as IRC+10420 and V509 Cas (Aret et al. 2017; Klochkova 2019), or by emission of warm molecular gas. The CO ro-vibrational bands are the most prominent molecular emission features. These molecular bands have been detected in the near-infrared spectra of a number of objects, such as the Galactic YHGs V509 Cas and ρ Cas (Lambert, Hinkle & Hall 1981; Gorlova et al. 2006; Kraus et al. 2022a), HD 179821 (Hrivnak, Kwok & Geballe 1994), [FMR2006] F15 (Davies et al. 2008; Kraus et al. 2023), and two objects in the Large Magellanic Cloud (LMC), the stars HD 269723 and HD 269953 (McGregor, Hillier & Hyland 1988; Oksala et al. 2013). Moreover, hot water vapour emission has recently been discovered from the environment of HD 269953 (Kraus et al. 2022b).

Outbursts in YHGs are usually identified by a sudden and steep decrease in visual brightness of the star along with indications for a rapid drop in spectroscopic temperature and the formation of TiO molecules in the expanding envelopes, which give rise to characteristic absorption bands in the spectra. The decrease in spectroscopic temperature makes the star to seemingly undergo a redward excursion in the HR diagram, until the episode of strong mass-loss cedes and the material expands and dilutes. The recovery phase is usually much longer than the onset of the outburst and proceeds with a gradual brightening, back to the object's pre-outburst magnitude, and an apparent heating up of the star causing its movement back to the hotter pre-outburst position in the HR diagram. The outburst duration of individual YHGs can be very different. Events have been recorded that lasted for decades as, for example, experienced by Var A in M33 (Humphreys et al. 2006) or for just a couple of years as for the Galactic star ρ Cas (Lobel et al. 2003; Kraus et al. 2019; Maravelias & Kraus 2022).

The cause of the outburst activity of YHGs has been ascribed in the literature to instabilities occurring in the envelope or atmosphere of the stars (e.g. Nieuwenhuijzen & de Jager 1995; de Jager et al. 2001). In particular, it has been proposed that, when a YHG approaches a temperature of ~ 7000 K, its atmosphere starts to become unstable leading to substantial mass-loss (e.g. Stothers & Chin 1993; de Jager et al. 2001; Lobel 2001; Stothers & Chin 2001). This temperature has been suggested to mark the lower boundary of a domain that has been dubbed the 'yellow evolutionary void' (Nieuwenhuijzen & de Jager 1995; de Jager & Nieuwenhuijzen 1997) because of the apparent lack of stars observable within this region. Furthermore, the outburst activity of YHGs has been referred to as bouncing at the yellow void (de Jager & Nieuwenhuijzen 1997) or, respectively, the yellow/white wall (Oudmaijer & de Wit 2013), because of the apparent redward-directed excursion the star undertakes after each event.

In this work, we critically review the concept of the dynamical instabilities, in particular the adiabatic instability that is usually claimed to be responsible for the outbursts and the mass ejections in YHGs. On the basis of an adiabatic stability analysis, we prove that all stellar models in the YHG domain are stable, questioning the existence of the yellow evolutionary void. Instead, we propose that the outbursts of YHGs could be related to strange mode instabilities. As has been shown by Gautschy & Glatzel (1990b) and Glatzel (1994), the excitation of these modes is to be expected in massive stars with high values of their luminosity over mass ratio, for which post-RSGs are excellent candidates (Saio, Georgy & Meynet 2013). Because strange mode instabilities have the potential to trigger time-variable mass-loss and mass ejections (Glatzel et al. 1999), they provide an excellent, alternative mechanism to drive outbursts in YHGs. We present a thorough stability analysis with respect to linear non-adiabatic radial perturbations focusing on the parameter space

occupied by confirmed YHGs. We demonstrate the occurrence of strange modes in all suitable models and show that their appearance does not (or only very mildly) depend on the effective temperature of the star.

In Section 2, the construction of stellar models and the basic assumptions and methods of the stability analysis are described. The results for models of ρ Cas and YHGs in the LMC together with an investigation of their dependence on effective temperature are presented in Section 3. Section 4 contains an extensive critical discussion in particular with respect to the common perception of adiabatic instability in the upper domain of the HR diagram. Our conclusions follow in Section 5.

2 ANALYSIS

2.1 Stellar models

In order to represent the observed properties of YHGs as accurately as possible, the study is based on envelope models constructed for the observed stellar parameter luminosity, effective temperature, and chemical composition. The uncertainty in mass is taken into account by considering wide mass ranges that should include the values suggested by both the spectroscopic analysis and the comparison with evolutionary models. In order to demonstrate the dependence on effective temperature of the results of the stability analyses, we shall also consider model sequences with varying effective temperature and fixed luminosity, chemical composition, and mass.

For prescribed luminosity, effective temperature, chemical composition, and mass, the structure of the stellar envelope between the photosphere and some suitably chosen bottom boundary can be determined by initial value integration of the equations of hydrostatic equilibrium, energy transport, and mass conservation, where unambiguous initial values are imposed at the photosphere. By definition, the luminosity is constant throughout the envelope. The bottom boundary is defined in terms of a maximum temperature that guarantees that nuclear burning does not prevail. It corresponds to a finite radius.

Concerning the treatment of convection, its onset is determined by Schwarzschild's criterion, standard mixing-length theory (Böhm-Vitense 1958) with 1.5 pressure scale heights for the mixing length is adopted for its description, and overshooting as well as semiconvection are disregarded. Opacities have been taken from the OPAL tables (see Rogers & Iglesias 1992, Iglesias & Rogers; 1996 and Rogers, Swenson & Iglesias 1996).

2.2 Stability analysis

In this study, we test the envelope models for YHGs for stability with respect to infinitesimal radial perturbations. The associated mathematical problem is derived and described (e.g. in Baker & Kippenhahn 1962). Adopting their notation and treating convection according to the 'frozen-in approximation' (see e.g. Baker & Kippenhahn 1965), the boundary eigenvalue problem posed by the analysis of radial linear non-adiabatic stellar stability and pulsations (linear non-adiabatic analysis, hereafter LNA analysis) is solved using the Riccati method (see Gautschy & Glatzel 1990a). In addition to the LNA analysis, the envelope models have been subject to a standard radial linear adiabatic stability analysis (for details, see Cox 1980).

As a result of the stability analyses, we obtain for each envelope model its complex eigenfrequencies σ , where the real parts σ_r correspond to the pulsation frequencies, and the imaginary parts σ_i indicate the growth or damping rates of the various modes. In

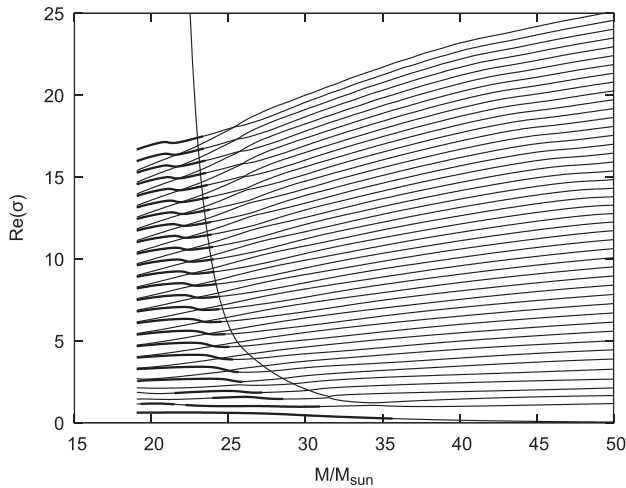


Figure 1. Real parts of the lowest order eigenfrequencies σ as a function of mass for envelope models with parameters resembling those of ρ Cas. Unstable modes are indicated by thick lines.

our normalization $\sigma_i > 0$ corresponds to damping (stability) and $\sigma_i < 0$ to growth and excitation (instability). For convenience, the eigenfrequencies will be presented in dimensionless form, i.e. they will be normalized by the global free-fall time (cf. Baker & Kippenhahn 1962; Gautschy & Glatzel 1990a). This normalization is common for theoretical studies such as the present investigation. In particular, it avoids the masking of results by the period–density relation.

In the radial linear adiabatic analysis (also referred to as the adiabatic approximation), the boundary eigenvalue problem is equivalent to a (self-adjoint) Sturm–Liouville problem (see e.g. Ledoux & Walraven 1958; Cox 1980). As a consequence, σ^2 is real and forms an infinite, well-ordered sequence with a smallest (fundamental) eigenvalue and a limit point at infinity in the adiabatic approximation. Thus, $\sigma^2 < 0$ for the fundamental eigenfrequency is a necessary and sufficient condition for instability (and vice versa) in the adiabatic approximation. Accordingly, adiabatic stability and instability can be determined by merely considering the fundamental adiabatic eigenfrequency. Instability sets in through $\sigma = 0$.

3 RESULTS

3.1 ρ Cas

Adopting observed values for the luminosity ($L = 5 \times 10^5 L_\odot$; Humphreys 1978), the mean spectroscopic effective temperature ($T_{\text{eff}} = 7000$ K; Lobel et al. 1994; Kraus et al. 2019), solar chemical composition [(X, Y, Z) = (0.74, 0.24, 0.02)], and a range in mass between 19 and $50 M_\odot$, including the most likely value of the star’s current evolutionary mass of $24.1 M_\odot$ (Kraus et al. 2019), a sequence of envelope models with the mass as a parameter has been constructed and tested for stability. Real and imaginary parts of the lowest order eigenfrequencies σ are presented as a function of mass in Figs 1 and 2.

At high masses, all modes are damped and their frequencies are regularly spaced, as expected for an ordinary acoustic resonator. With decreasing mass (below $\approx 35 M_\odot$), multiple mode crossings and mode pairings unfolded both according to the ‘avoided crossing’ and the ‘instability band’ coupling schemes (see e.g. Gautschy &

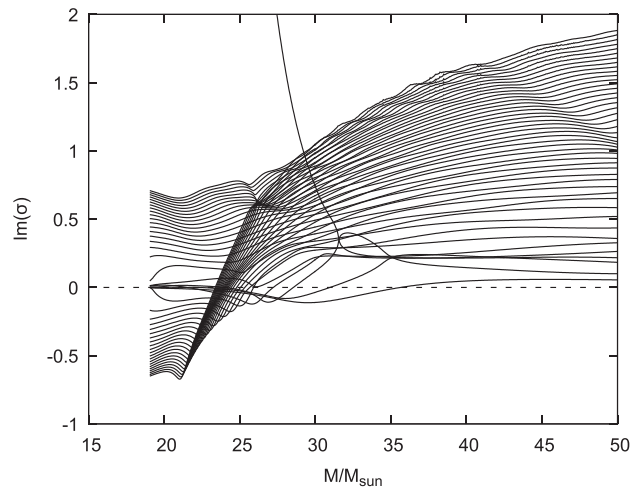


Figure 2. Imaginary parts of the lowest order eigenfrequencies σ as a function of mass for envelope models with parameters resembling those of ρ Cas.

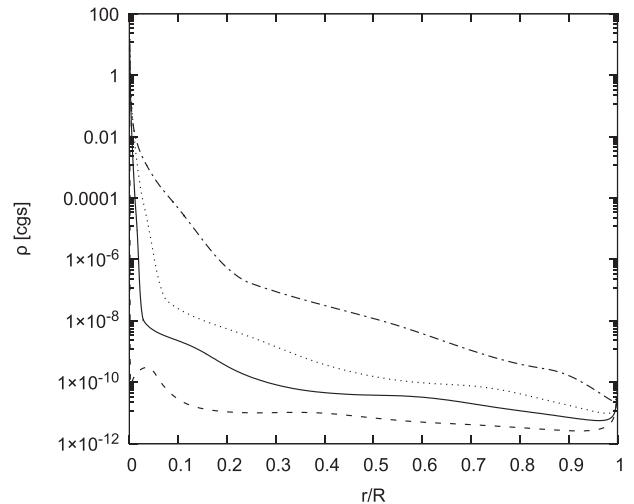


Figure 3. The density ρ as a function of relative radius for envelope models with chemical composition (X, Y, Z) = (0.74, 0.24, 0.02), luminosity $L = 5 \times 10^5 L_\odot$, effective temperature $T_{\text{eff}} = 7000$ K, and the masses $M = 24.1 M_\odot$ (full line), $M = 19.1 M_\odot$ (dashed line), $M = 30 M_\odot$ (dotted line), and $M = 50 M_\odot$ (dash-dotted line). Note that the bottom boundary of the models corresponds to a finite radius.

Glatzel 1990b) are found, which are associated with the occurrence of instabilities having growth rates in the dynamical regime. Apart from one strongly damped mode, whose frequency and damping increases, frequencies and dampings tend to decrease with decreasing mass. For masses below $\approx 25 M_\odot$, damped and unstable modes exhibit an approximately complex conjugate symmetry, which is typical for the pure form of mode coupling according to the ‘instability band’ scheme.

The behaviour of modes and the occurrence of instabilities is a consequence of the change with mass of the stellar structure. The latter is shown in Fig. 3 by means of the density stratification of envelope models for ρ Cas with four different masses.

The core–envelope structure of these models, where a small core contains almost the total mass of the star and a tenuous envelope with

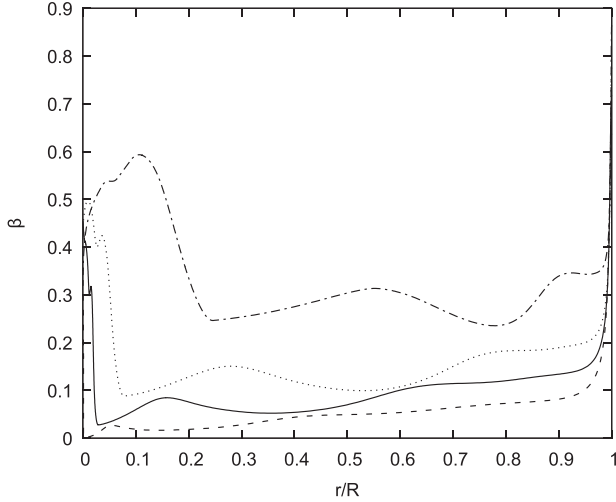


Figure 4. The ratio β of gas pressure to total pressure as a function of relative radius for envelope models with chemical composition $(X, Y, Z) = (0.74, 0.24, 0.02)$, luminosity $L = 5 \times 10^5 L_\odot$, effective temperature $T_{\text{eff}} = 7000$ K, and the masses $M = 24.1 M_\odot$ (full line), $M = 19.1 M_\odot$ (dashed line), $M = 30 M_\odot$ (dotted line), and $M = 50 M_\odot$ (dash-dotted line). Note that the bottom boundary of the models corresponds to a finite radius.

negligible contribution to the stellar mass covers the entire space, is becoming more and more pronounced as the mass decreases. This change in structure, in particular the decrease of density in the envelope with decreasing mass, has a direct impact on the contribution of gas pressure to total pressure in the stellar envelope. The ratio β of gas pressure to total pressure for the models considered is presented in Fig. 4.

Whereas for $M = 50 M_\odot$ the fraction of gas pressure is still higher than 25 percent everywhere, it falls below 10 percent in almost the entire envelope for $M = 19.1 M_\odot$. Thus, the envelopes studied become more and more dominated by radiation pressure as the mass decreases. Another crucial consequence of the structure and low densities of the envelopes considered refers to the time-scales governing acoustic waves in the stellar envelope [see also the analogue discussions in Gautschy & Glatzel (1990b) and Glatzel (2021)].

The local dynamical time-scale may be estimated as the time needed by a sound wave to cross a mass shell with thickness Δr . Estimating the sound speed as $c^2_{\text{Sound}} \propto p/\rho$ (p : pressure, ρ : density), it is given by

$$\tau_{\text{Dyn}} \propto \Delta r \sqrt{\rho/p}. \quad (1)$$

On the other hand, the local thermal time-scale of a mass shell with mass Δm may be defined as the time needed to radiate its thermal energy content at the local luminosity, where the thermal energy content might be expressed as the product of the specific heat c_p , the temperature T , and the mass Δm . Rewriting the latter in terms of the density ρ and the volume of the mass shell, we finally obtain for the local thermal time-scale:

$$\tau_{\text{Thermal}} \propto \frac{c_p T \Delta m}{L} = \frac{c_p T \rho 4\pi r^2 \Delta r}{L}. \quad (2)$$

Both the local dynamical and the local thermal time-scale depend on the thickness Δr of the mass shell considered. Unless there are further arguments how to choose Δr , they can be given any value since the choice of Δr is ambiguous. Thus, the local dynamical and thermal time-scales given by equations (1) and (2) are ill-defined

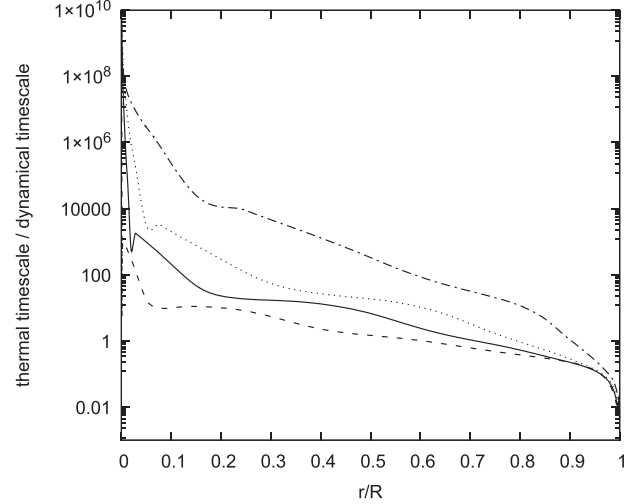


Figure 5. The ratio of thermal and dynamical time-scales as a function of relative radius for envelope models with chemical composition $(X, Y, Z) = (0.74, 0.24, 0.02)$, luminosity $L = 5 \times 10^5 L_\odot$, effective temperature $T_{\text{eff}} = 7000$ K, and the masses $M = 24.1 M_\odot$ (full line), $M = 19.1 M_\odot$ (dashed line), $M = 30 M_\odot$ (dotted line), and $M = 50 M_\odot$ (dash-dotted line). Note that the bottom boundary of the models corresponds to a finite radius.

quantities without any physical relevance. However, their ratio being independent of Δr is well defined and given by

$$\frac{\tau_{\text{Thermal}}}{\tau_{\text{Dyn}}} \propto \frac{4\pi r^2 \rho c_p T}{L} \sqrt{p/\rho}. \quad (3)$$

The ratio of thermal and dynamical time-scales as a function of relative radius for the envelope models discussed is shown in Fig. 5. As in any stellar model, this ratio achieves very high values in the core and is smallest (maybe even below unity) at the surface. As a consequence, all sound waves become adiabatic in the deep interior of the star and non-adiabatic effects have to be taken into account in a certain domain below the stellar surface, where the ratio of thermal and dynamical time-scales is of order unity or smaller. This domain depends on the stellar model and shrinks with increasing mass for the models discussed (see Fig. 5). In other words, with decreasing mass we expect the adiabatic approximation to become less and less valid. Instead of characterizing them by an infinite thermal time-scale (adiabatic approximation), low-mass models for ρ Cas should rather be described by the opposite approximation of a small or vanishing thermal time-scale. The latter corresponds to the non-adiabatic reversible (NAR) approximation (see e.g. Gautschy & Glatzel 1990b).

In the NAR approximation, eigenfrequencies occur in complex conjugate pairs, i.e. modes are either neutrally stable or damped and unstable modes appear simultaneously thus forming pairs with the same frequency and identical moduli of growth and damping rates. Motivated by the consideration that the NAR approximation might be applicable to low-mass models for ρ Cas, we have performed a corresponding analysis whose results are shown in Figs 6 and 7.

In the NAR approximation, for high masses the modes are found to be neutrally stable. With decreasing mass below $\approx 25 M_\odot$ some of the adjacent modes merge to form complex conjugate pairs of damped and unstable modes in a way that is quite close to the analysis without approximation (cf. Figs 1 and 2). For comparison, Fig. 8 contains the imaginary parts of σ both from the exact and the NAR analysis. With respect to the strong dynamical instabilities at low

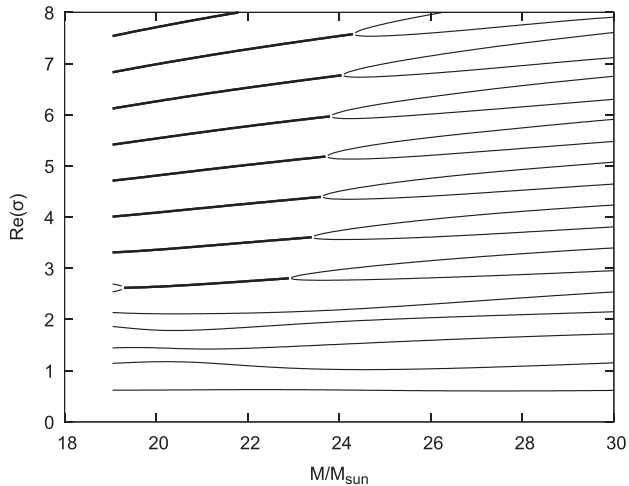


Figure 6. Same as Fig. 1, but using the NAR approximation. Thin lines correspond to neutrally stable modes and thick lines to complex conjugate pairs of damped and unstable modes.

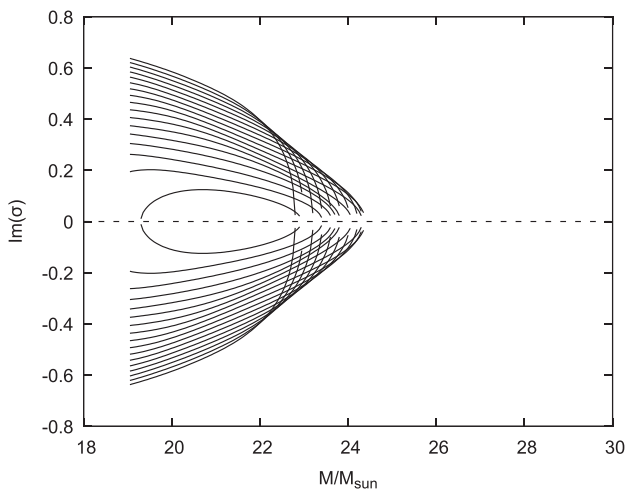


Figure 7. Same as Fig. 2, but using the NAR approximation. Modes are either neutrally stable or appear in complex conjugate pairs of damped and unstable modes.

masses, their complex conjugate symmetry, and the associated mode interactions, we conclude that the NAR approximation provides at least qualitatively satisfactory results. These findings thus also support the assumption that the opposite approximation of an infinite thermal time-scale, the adiabatic approximation, should be invalid for the models considered.

To prove this conjecture, an adiabatic analysis has been performed for the ρ Cas models. The results in terms of the frequencies of the three lowest neutrally stable adiabatic modes are shown and compared with the exact frequencies in Fig. 9. From Fig. 9, we deduce that – as expected – the adiabatic frequencies do not provide an approximation to the exact frequencies in any respect, not even for high masses. Moreover, the fundamental adiabatic mode that indicates adiabatic stability and instability, respectively, exhibits finite frequency for all models and thus no evidence at all for adiabatic instability.

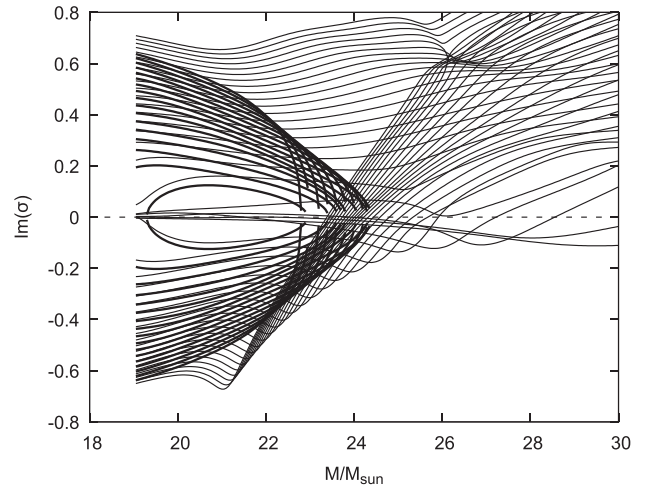


Figure 8. Same as Figs 2 and 7, but with results from the exact analysis (thin lines) and using the NAR approximation (thick lines) superimposed. Note the similarity of exact and NAR results in particular in the domain of strong instabilities with growth rates in the dynamical regime.

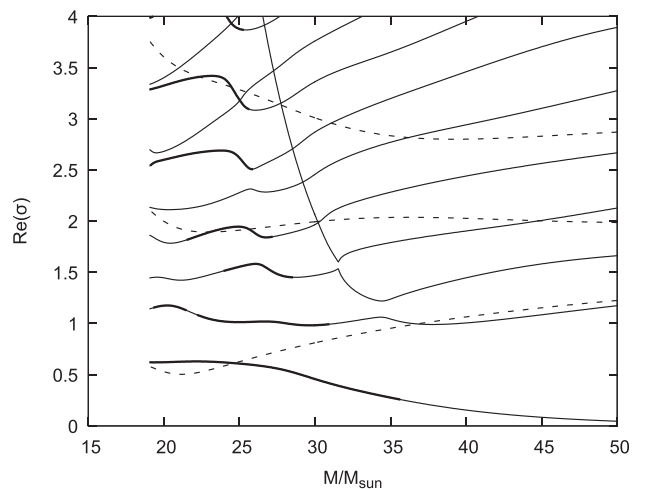


Figure 9. Same as Fig. 1, but with the three lowest neutrally stable adiabatic eigenfrequencies (dashed lines) added. We emphasize that there is no instability in the adiabatic approximation and the adiabatic frequencies do not appear to provide an approximation to the correct frequencies at all.

To complete the discussion of the adiabatic analysis, the adiabatic exponent γ_{ad} is shown for four ρ Cas models with different mass in Fig. 10. All models exhibit zones in which γ_{ad} falls below the critical value $4/3$. They are associated with the various ionization processes, each of them causing a minimum of γ_{ad} . Even if these zones with $\gamma_{\text{ad}} < 4/3$ do exist, their strength is not sufficient for adiabatic instability, i.e. the pressure-weighted volumetric mean of γ_{ad} does not fall below $4/3$ (which would be sufficient for adiabatic instability). The fact that the fundamental mode has not shown any evidence for instability explicitly proves that the correct mean of γ_{ad} is bigger than $4/3$. Outside the ionization zones, γ_{ad} is bigger than but close to $4/3$ and increases with mass. This is a consequence of dominant radiation pressure (cf. Fig. 4): The limit of pure radiation pressure ($\beta \rightarrow 0$) implies $\gamma_{\text{ad}} \rightarrow 4/3$. With increasing mass, β increases (see Fig. 4) and, together with it, also γ_{ad} .

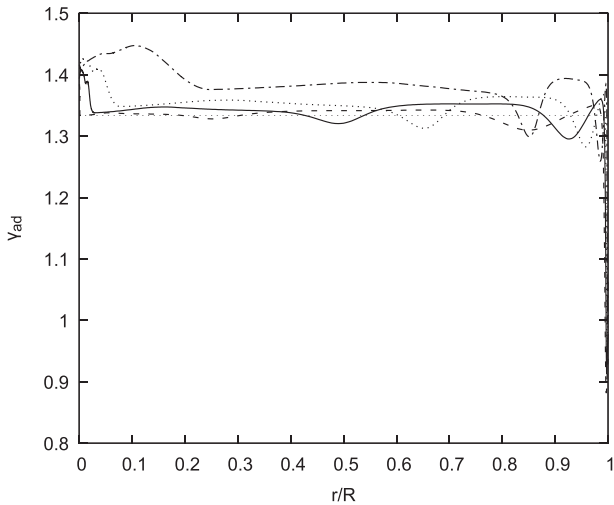


Figure 10. The adiabatic exponent γ_{ad} as a function of relative radius for envelope models with chemical composition $(X, Y, Z) = (0.74, 0.24, 0.02)$, luminosity $L = 5 \times 10^5 L_{\odot}$, effective temperature $T_{\text{eff}} = 7000$ K, and the masses $M = 24.1 M_{\odot}$ (full line), $M = 19.1 M_{\odot}$ (dashed line), $M = 30 M_{\odot}$ (dotted line), and $M = 50 M_{\odot}$ (dash-dotted line). Note that the bottom boundary of the models corresponds to a finite radius.

3.2 Yellow hypergiants in the LMC

In this section, the dependence on metallicity of instabilities in the YHG domain will be studied. This is motivated by the recent investigations of Kourniotis et al. (2022) of evolved hypergiants in the LMC who classified the star HD 269723 as a luminous post-RSG and HD 271182 as a ρ Cas analogue and thus both as YHGs. These objects hence serve as ideal targets for our analysis. Both stars have a similar temperature of $T_{\text{eff}} \sim 6000$ K but different luminosities. Kourniotis et al. (2022) have derived values of $L = 4.5 \times 10^5 L_{\odot}$ and $L = 6 \times 10^5 L_{\odot}$ for HD 271182 and HD 269723, respectively. With these luminosities, the initial and current evolutionary masses of the stars fall into the ranges of 32–40 and 20–30 M_{\odot} . We adopt an effective temperature of $T_{\text{eff}} = 6000$ K, the two luminosity values, and the chemical composition $(X, Y, Z) = (0.75, 0.24, 0.01)$ resembling that of LMC objects. With respect to the uncertainty of mass, two sequences of envelope models with the mass as a parameter have been constructed and tested for stability. For the sequence with luminosity $L = 4.5 \times 10^5 L_{\odot}$, real and imaginary parts of the lowest order eigenfrequencies σ are presented as a function of mass in Figs 11 and 12.

Figs 11 and 12 may be compared with their counterparts for ρ Cas, Figs 1 and 2. Qualitatively, there is no difference between the results for ρ Cas and the LMC object. Mode interactions and associated instabilities do occur in the same way for both sequences. Instability sets in below $\approx 30 M_{\odot}$ for the LMC object, at a somewhat lower mass than for ρ Cas, which is likely to be due to its smaller luminosity. As for ρ Cas, we have performed an adiabatic analysis for the LMC models. Its result for the sequence with $L = 4.5 \times 10^5 L_{\odot}$ in terms of the three lowest neutrally stable adiabatic eigenfrequencies is shown and compared with the exact results in Fig. 13 (cf. the counterpart for ρ Cas, Fig. 9). Except for the fundamental adiabatic mode at high masses, the adiabatic frequencies do not provide an approximation to the correct frequencies. Moreover, we emphasize that an adiabatic instability does not exist.

The results obtained for the sequence with $L = 6 \times 10^5 L_{\odot}$ are very similar to those for its counterpart with $L = 4.5 \times 10^5 L_{\odot}$, such that a

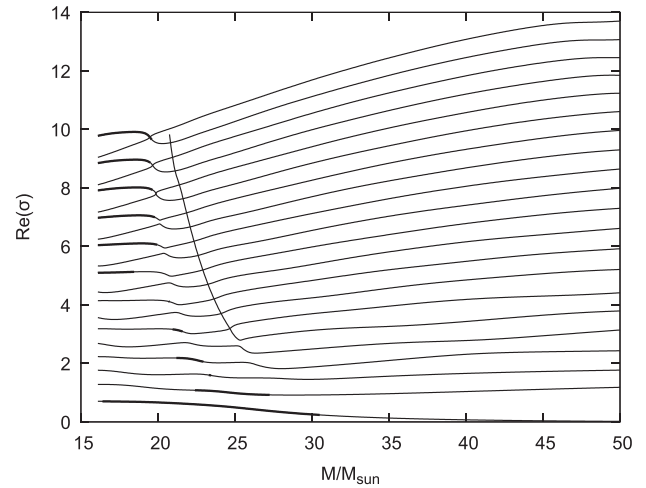


Figure 11. Real parts of the lowest order eigenfrequencies σ as a function of mass for envelope models with luminosity $L = 4.5 \times 10^5 L_{\odot}$, effective temperature $T_{\text{eff}} = 6000$ K, and chemical composition $(X, Y, Z) = (0.75, 0.24, 0.01)$ resembling that of LMC objects. Unstable modes are indicated by thick lines.

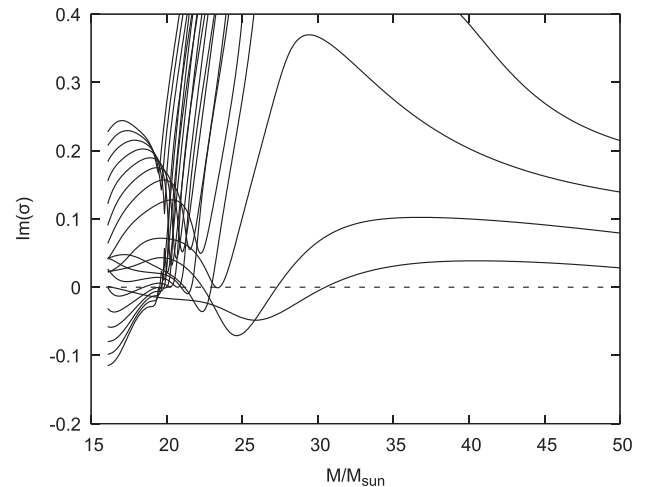


Figure 12. Imaginary parts of the lowest order eigenfrequencies σ as a function of mass for envelope models with luminosity $L = 4.5 \times 10^5 L_{\odot}$, effective temperature $T_{\text{eff}} = 6000$ K, and chemical composition $(X, Y, Z) = (0.75, 0.24, 0.01)$ resembling that of LMC objects.

separate discussion is redundant. Accordingly, for this sequence we only show the imaginary parts of σ as a function of mass in Fig. 14. As a consequence of the higher luminosity, the upper limit in mass for instability has shifted to higher masses (to around $\approx 40 M_{\odot}$, compare Figs 12 and 14).

3.3 Dependence on effective temperature of instability

In this section, the dependence on effective temperature of the instabilities found in the YHG domain will be studied. For this purpose, sequences of envelope models with the effective temperature as a parameter covering the range between red supergiant and blue supergiant (BSG) are constructed and tested for stability. Adopting the chemical composition $(X, Y, Z) = (0.74, 0.24, 0.02)$, the various sequences are characterized by the values selected for

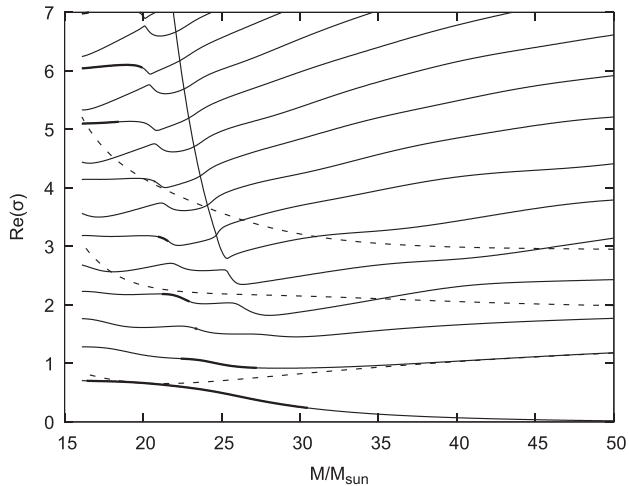


Figure 13. Same as Fig. 11, but with the three lowest neutrally stable adiabatic eigenfrequencies (dashed lines) added. We emphasize that there is no instability in the adiabatic approximation and the adiabatic frequencies do not appear to provide an approximation to the correct frequencies at all.

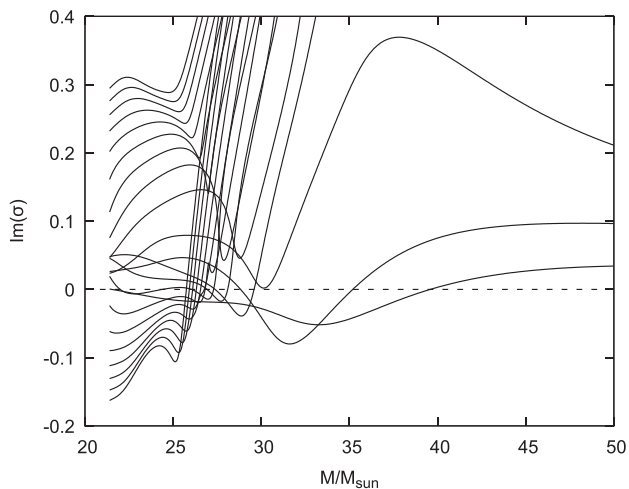


Figure 14. Same as Fig. 12, but for envelope models with a higher luminosity ($L = 6 \times 10^5 L_\odot$).

mass and luminosity. For a sequence with luminosity $L = 5 \times 10^5 L_\odot$ and mass $M = 25 M_\odot$, real and imaginary parts of the lowest order eigenfrequencies σ are presented as a function of effective temperature in Figs 15 and 16. In addition to the non-adiabatic LNA analysis, also an adiabatic analysis has been performed. Its result, i.e. the frequencies of the two lowest neutrally stable adiabatic eigenfrequencies is also shown in Fig. 15.

Figs 15 and 16 demonstrate that the mode interactions and associated instabilities with growth rates in the dynamical regime identified in the YHG domain persist for the entire effective temperature range from red to blue supergiants. Whether the stable gap around $\log T_{\text{eff}} \approx 3.7$ is significant, remains to be seen. Again, the adiabatic eigenfrequencies do not provide an approximation to the exact frequencies in any respect, as the adiabatic approximation does not apply. We emphasize that for the entire range of effective temperatures studied adiabatic instability does not exist. The treatment of dominant convection in particular the coupling of strong convection

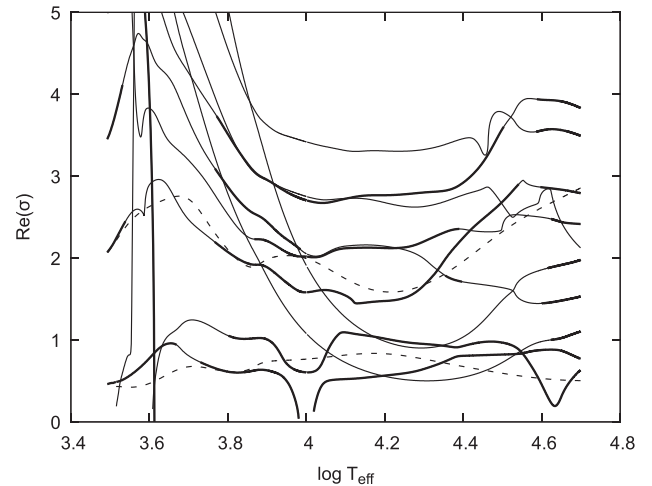


Figure 15. Real parts of the lowest order eigenfrequencies σ as a function of effective temperature for envelope models with luminosity $L = 5 \times 10^5 L_\odot$, mass $M = 25 M_\odot$, and chemical composition $(X, Y, Z) = (0.74, 0.24, 0.02)$. Unstable modes are indicated by thick lines. Dashed lines correspond to the two lowest neutrally stable adiabatic eigenfrequencies.

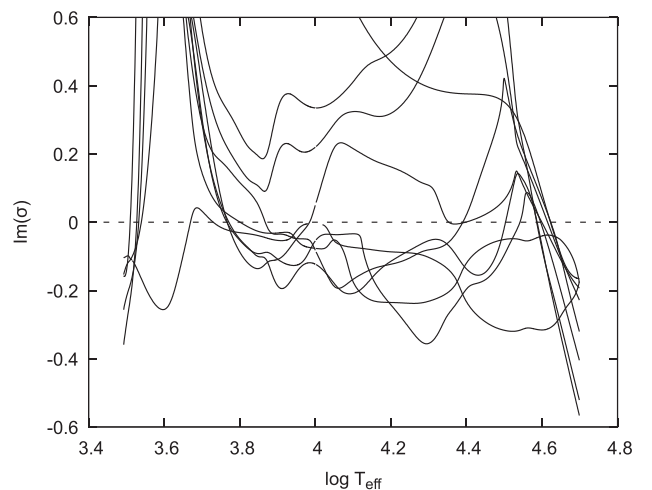


Figure 16. Imaginary parts of the lowest order eigenfrequencies σ as a function of effective temperature for envelope models with luminosity $L = 5 \times 10^5 L_\odot$, mass $M = 25 M_\odot$, and chemical composition $(X, Y, Z) = (0.74, 0.24, 0.02)$.

and pulsation is still an unsolved problem and becomes important at the low-temperature end of the model sequence. With respect to these uncertainties, the results in the RSG domain should be interpreted with caution.

With regard to the controversial discussion of adiabatic instability of massive stars in the BSG and luminous blue variable (LBV) phase (see Glatzel & Kiriakidis; 1998 and Stothers; 1999), we have performed an adiabatic analysis for additional sequences of envelope models. For four sequences, the results in terms of the lowest order adiabatic eigenfrequencies as a function of effective temperature are shown in Figs 17 and 18. σ^2 is real and remains positive in any case. Thus, all modes are neutrally stable and an adiabatic instability does not exist. The sequences of avoided crossings appearing at high effective temperatures in Fig. 17 are caused by the crossing of two

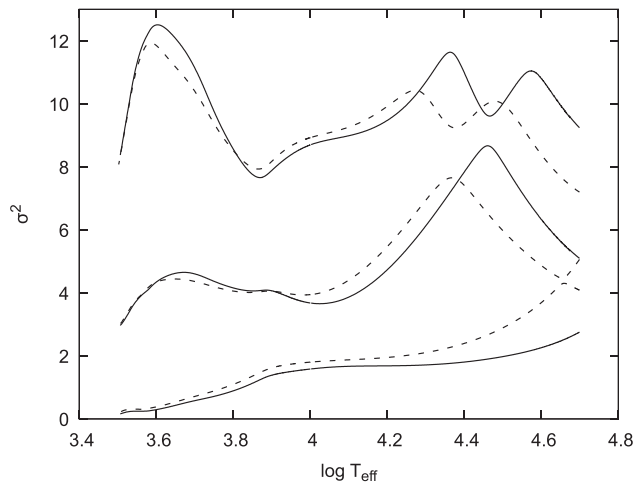


Figure 17. The real and positive square σ^2 of the three lowest neutrally stable adiabatic eigenfrequencies as a function of effective temperature for envelope models with chemical composition $(X, Y, Z) = (0.74, 0.24, 0.02)$, luminosity $L = 10^6 L_\odot$ and mass $M = 70 M_\odot$ (full lines). Dashed lines represent the eigenfrequencies for envelope models with luminosity $L = 5 \times 10^5 L_\odot$ and mass $M = 45 M_\odot$.

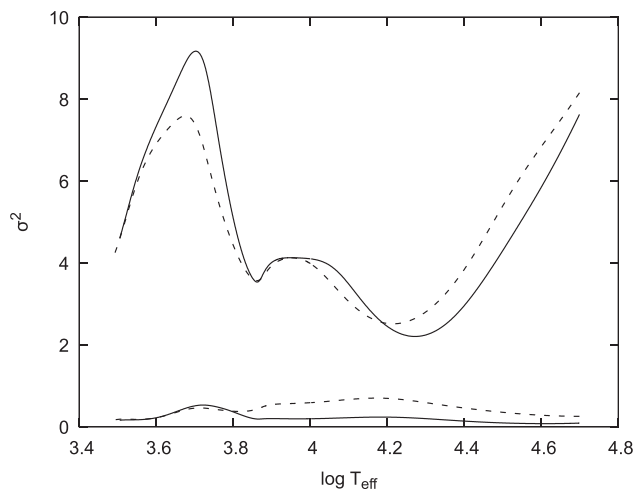


Figure 18. The real and positive square σ^2 of the two lowest neutrally stable adiabatic eigenfrequencies as a function of effective temperature for envelope models with chemical composition $(X, Y, Z) = (0.74, 0.24, 0.02)$, luminosity $L = 10^6 L_\odot$ and mass $M = 40 M_\odot$ (full lines). Dashed lines represent the eigenfrequencies for envelope models with luminosity $L = 5 \times 10^5 L_\odot$ and mass $M = 25 M_\odot$.

sets of acoustic modes associated with two acoustic cavities in the stellar envelope and have been discussed, e.g. by Kiriakidis, Fricke & Glatzel (1993) and Glatzel & Kiriakidis (1998).

4 DISCUSSION

4.1 Non-adiabatic stability analysis

The study of the stability of massive stars in the vicinity of the Humphreys–Davidson limit dates back to the investigation of Glatzel & Kiriakidis (1993), where violent instabilities with growth rates in the dynamical range have been identified. These

instabilities have been found to be associated with mode coupling and the apparent occurrence of additional unexpected, until then incomprehensible modes, which were addressed as ‘strange modes’, the associated instabilities as ‘strange mode instabilities’. With the arrival of new opacities that correctly account for the contribution of heavy elements (Rogers & Iglesias 1992), the study by Glatzel & Kiriakidis (1993) has been repeated by Kiriakidis et al. (1993) on the basis of these opacities with similar results for effective temperatures below $\approx 20\,000$ K. For higher effective temperatures, additional metallicity-dependent strange mode instabilities have been identified. The boundary in the HR diagram, above which all stellar models independent of metallicity exhibit violent strange mode instabilities with growth rates in the dynamical regime, was found to coincide with the observed Humphreys–Davidson limit. Meanwhile, the investigations have been confirmed several times and strange mode instabilities are in general expected to occur, if the luminosity-to-mass ratio (in solar units) exceeds values around $\approx 10^4$ (see e.g. Saio 2011).

According to the previous studies, strange mode instabilities are to be expected for the models of YHG considered here, as their luminosity-to-mass ratio (in solar units) is of the order of $\approx 10^4$. In fact, the multiple mode couplings associated with violent instabilities that have been discussed in the previous sections correspond to strange modes and strange mode instabilities. That certain sequences of mode interactions may create the impression of additional ‘strange’ modes, has been described by Gautschy & Glatzel (1990b) and may be seen in Fig. 15, where the eigenfrequencies are presented as a function of effective temperature rather than as function of mass. However, not all ‘strange modes’ are caused by mode coupling processes. For example, the mode with the lowest frequency at $M = 50 M_\odot$ in Fig. 1 and strongly increasing frequency and damping rate for decreasing mass, belongs to the thermal rather than to the acoustic spectrum. This classification is suggested by considering the thermal time-scale, being small for low masses and increasing with mass (cf. Fig. 5). Consequently, thermal frequencies should decrease with mass, as seen for the mode discussed. Note that around $\approx 35 M_\odot$ the thermal mode interacts with the acoustic spectrum through avoided crossings, which for the lowest acoustic mode is not very well pronounced.

Another indication for the presence of thermal modes is found in Figs 15 and 16. Around $\log T_{\text{eff}} \approx 4$, both the real and imaginary part of the lowest order mode approach zero thus suggesting a classification as a thermal mode at least in a gap around $\log T_{\text{eff}} \approx 4$. Across this gap the mode has not been followed continuously, since multiple interactions with thermal modes close to zero frequency make an unambiguous continuous tracking extremely difficult. Moreover, for the models considered the thermal spectrum is not decisive for stellar stability, even though its study may be of academic interest.

4.2 Adiabatic stability analysis

Due to short thermal time-scales for large fractions of the considered stellar envelopes (see Fig. 5), the adiabatic analysis is invalid and has been found not to provide a satisfactory approximation to the exact results in any respect. Moreover, none of the models studied exhibits an adiabatic instability. As a value below $4/3$ of the mean of the pressure-weighted volumetric mean of the adiabatic exponent is a sufficient condition for instability (see Ledoux & Walraven 1958), this result strictly proves that the mean adiabatic index stays above $4/3$ in any case. We note that the primary procedure to test adiabatic stability consists of calculating the (real) square σ^2 of the fundamental adiabatic eigenfrequency σ . Its sign provides a

necessary and sufficient condition for adiabatic stability: For $\sigma^2 < 0$, we have instability, otherwise stability. In this study, we have applied this method. A secondary procedure providing a sufficient condition for instability only is based on the Rayleigh–Ritz variational principle associated with the differential adiabatic perturbation problem (see Ledoux & Walraven; 1958 and Glatzel & Kiriakidis; 1998). It allows for an estimate of an upper bound for σ^2 of the adiabatic fundamental mode, whose sign is determined by $3\langle\gamma_{\text{ad}}\rangle - 4$, where $\langle\gamma_{\text{ad}}\rangle$ denotes the pressure-weighted volumetric mean of γ_{ad} over the entire stellar model. Thus, $\langle\gamma_{\text{ad}}\rangle < 4/3$ is a sufficient but not necessarily necessary condition for instability. We emphasize that for the mean of the adiabatic exponent the entire stellar model has to be taken into account and that the domain for calculating the mean cannot be chosen arbitrarily. Otherwise $\langle\gamma_{\text{ad}}\rangle$ could be given any arbitrary value (see Fig. 10).

Our results concerning adiabatic stability are in blatant contradiction to the common perception of instability regions in the upper HR diagram (see e.g. de Jager et al. 2001; Stothers & Chin 2001). The prevailing opinion assumes that two domains of adiabatic instability exist, where the ‘blue’ domain accommodates the LBVs and the ‘yellow–red’ domain the YHGs. Apart from Stothers & Chin (2001) whose study reportedly is based on an explicit solution of the adiabatic wave equation, all other studies rely on a consideration of the mean adiabatic exponent for the determination of the domains of instability.

With respect to the ‘blue’ instability domain, we have already contradicted the common view in an earlier paper (Glatzel & Kiriakidis 1998) by (a) arguing that the adiabatic approximation is not valid at all due to short thermal time-scales in the stellar envelope and by (b) explicitly demonstrating that there is no adiabatic instability. Thus, the arguments raised here are not new and have been produced already in earlier studies in a similar context.

4.3 The relation between non-adiabatic and adiabatic stability analysis

Concerning the objections raised in Glatzel & Kiriakidis (1998), comments were published by Stothers (1999), which also form the basis of the study by de Jager et al. (2001). According to Stothers (1999), adiabatic stability and non-adiabatic stability are considered separately and independently. We strongly disagree, since the adiabatic analysis is an approximation and subordinate to the non-adiabatic analysis, which can only be applied if the thermal time-scales tend to infinity. It depends on the stellar model, whether a complete non-adiabatic analysis is required or the adiabatic analysis is sufficient. For massive stars having short thermal time-scales in their envelopes, the adiabatic approximation is not valid and the appropriate analysis must take thermal effects into account. There is no choice concerning the analysis, and the two approaches (non-adiabatic and adiabatic analyses) cannot be applied independently and separately. In particular, it is meaningless to distinguish between dynamical and pulsational instability. Note that in our studies the term ‘dynamical’ only refers to the time-scale and not to the type or mechanism of an instability. In the notation of Stothers (1999), it seems that the term ‘dynamical instability’ is also used as an equivalent for ‘adiabatic instability’. Thus, we conclude that an adiabatic stability analysis for the massive stars considered is irrelevant. Compared to this, the fact that we do not find adiabatic instabilities is of minor importance. An explanation for the discrepancy is not presented by Stothers (1999).

4.4 Criteria for adiabatic instability and their derivation

In general, the criterion for adiabatic instability involving the adiabatic exponent is derived from the Rayleigh–Ritz variational principle associated with the differential adiabatic perturbation problem (see Ledoux & Walraven 1958; Glatzel & Kiriakidis 1998). Stothers (1999) presents an alternative derivation providing the same instability criterion as a result. It is based on an integral relation for the eigenfrequency (equation 2 of Stothers 1999), which may be derived either from the virial theorem or from an integration of the adiabatic wave equation (see Ledoux & Walraven 1958). Contrary to the Rayleigh–Ritz variational principle, this relation is not quadratic but linear in the Lagrangean displacement, which here is to be regarded as a solution of the wave equation rather than as a test function of the variational principle. A simple inspection of the wave equation shows that for $\gamma_{\text{ad}} = 4/3$ and $\sigma^2 = 0$, a constant Lagrangean displacement provides a solution of the perturbation problem. Stothers (1999) verifies this by numerical calculation and suggests to insert a Heaviside function for the Lagrangean displacement in his integral relation (2) for σ^2 . Integration by parts then leads to a relation (equation 3 of Stothers 1999), apparently similar to that obtained from the Rayleigh–Ritz formalism (see e.g. equation A4 of Glatzel & Kiriakidis 1998), which forms the basis of the adiabatic instability criterion. In his derivation, Stothers (1999) inserts a Heaviside function for the solution of the wave equation in relation (2), which holds only for $\gamma_{\text{ad}} \approx 4/3$ and $\sigma^2 \approx 0$. For the latter, relations (2) and (3) are in fact identically satisfied. However, ignoring and relaxing the initial assumptions $\gamma_{\text{ad}} \approx 4/3$ and $\sigma^2 \approx 0$ (which guarantee the Heaviside function as a solution of the wave equation), to derive a relation for $\gamma_{\text{ad}} \neq 4/3$ and $\sigma^2 \neq 0$, implies a contradiction. Accordingly, even if the result appears to be correct, we consider its derivation to be wrong.

4.5 Comparison with observable quantities

For a comparison with observable quantities it might be tempting to convert the dimensionless frequencies derived here into pulsation periods and e-folding times. However, we emphasize that this study is entirely based on a linear analysis that does not allow for a determination of amplitudes. Therefore, e-folding times can, in principle, not be related to any observed light variations, even if there might be a tendency that final amplitudes reached in the non-linear regime increase with the growth rate of the underlying instability (see e.g. Grott, Chernigovski & Glatzel 2005).

Non-linear simulations of strange mode instabilities have shown (see e.g. Glatzel 2009) that due to their strength the stellar envelope is inflated by successive shock waves. As a consequence, the pulsation period increases and finally is significantly larger than the period determined by the linear analysis. We expect this behaviour also for the strange mode instabilities in YHGs, except possibly for models close to the onset of instability, where the growth rates are small. Accordingly, a comparison of linear periods with observed periods must be treated with caution.

Taking these cautionary remarks into account, the dimensionless frequencies σ can be converted into pulsation periods P and e-folding times τ_e by

$$P = \frac{2\pi}{\sigma_r} \sqrt{\frac{R^3}{3GM}} \quad (4)$$

and

$$\tau_e = \frac{1}{\sigma_i} \sqrt{\frac{R^3}{3GM}}, \quad (5)$$

where R denotes the stellar radius and G is the gravitational constant. Equation (4) represents the period–density relation and contains the global dynamical time-scale that may be expressed as

$$\sqrt{\frac{R^3}{3GM}} = 23.2 \text{ d} \left(\frac{L}{5 \times 10^5 L_{\odot}} \right)^{3/4} \left(\frac{T_{\text{eff}}}{7000 \text{ K}} \right)^{-3} \left(\frac{M}{25 M_{\odot}} \right)^{-1/2}. \quad (6)$$

Using equations (4) and (6), we obtain from Fig. 1 theoretical pulsation periods for ρ Cas in the range between approximately 16 and 292 d. Noteworthy, the latter agrees considerably well with cyclic photometric variability of 200–300 d reported for ρ Cas over the past decades (Zsoldos & Percy 1991; Percy, Kolin & Henry 2000; Kraus et al. 2019). Moreover, the models for stars with LMC metallicity (Fig. 11) predict periods of about 750 d from the lowest order eigenfrequency for stars with about $30 M_{\odot}$, which is similar to the dominant period derived by Kournotis et al. (2022) from the photometric light curves of the two LMC objects HD 269723 (800 d) and HD 271182 (833 d).

5 CONCLUSIONS

We have investigated the stability of stellar models in the YHG domain with respect to infinitesimal radial perturbations. For luminosity-to-mass ratios above $\approx 10^4$, violent strange mode instabilities with growth rates in the dynamical regime have been identified. Adopting the luminosities and masses derived from observations, we thus predict YHGs to suffer from these instabilities. For luminosity-to-mass ratios above $\approx 10^4$, the strange mode instabilities persist over the entire range of effective temperatures from RSGs to BSGs, except possibly for a small stable gap around $\log T_{\text{eff}} \approx 3.7$. Whether this gap is significant remains to be studied. Should it be relevant for stellar evolution, it could mean that stars are forced to evolve into this gap, and may be pushed back into the gap once they try to evolve into the surrounding unstable domains.

The envelopes of YHGs with a pronounced core envelope structure are characterized by short thermal time-scales and dominant radiation pressure, which according to a model for strange mode instabilities by Glatzel (1994) are essential ingredients for the occurrence of strange mode instabilities. In accordance with the short thermal time-scales, the NAR approximation (vanishing thermal time-scale) has been found to describe mode interactions and instabilities at least qualitatively correct, when compared with the exact results. In contrast to the NAR approximation, the opposite approximation of infinite thermal time-scale (adiabatic approximation), as expected, does not provide an approximation to the exact results in any respect. We emphasize that due to the short thermal time-scales in YHG envelopes a non-adiabatic analysis is mandatory and an adiabatic analysis is irrelevant.

According to the common perception, adiabatic instability causes instability regions in the upper HR diagram that also cover the YHG domain. Therefore, we have performed an adiabatic analysis for YHG models, even if the short thermal time-scales indicate that the adiabatic approximation does not hold there. Contrary to the prevailing opinion, our results do not exhibit any adiabatic instability. Thus, we disagree with the common conception in two respects: (i) the adiabatic approximation is not applicable and (ii) even if the adiabatic approximation was applicable, there is no adiabatic instability.

The linear analyses performed here provide information neither on the amplitude that an unstable perturbation may reach, nor on the final fate of an unstable object. To determine them, the evolution

of instabilities into the non-linear regime needs to be followed by numerical simulation. For strange mode instabilities in massive stars, such simulations (see e.g. Glatzel et al. 1999; Grott et al. 2005) indicate that pulsationally driven mass-loss may be a consequence of the instability. Currently, we are performing corresponding numerical simulations for YHG models, which we expect to provide information about whether strange mode instabilities can contribute to the observed mass-loss and outbursts of these stars. Their results will be commented on in a subsequent paper.

Strange mode instabilities are not restricted to radial perturbations and occur also for non-radial perturbations in a similar way for low harmonic degrees l up to $l \approx 300$ (see e.g. Glatzel & Gautschy 1992; Glatzel & Mehren 1996; Glatzel & Kaltschmidt 2002). Thus, we expect non-radial strange mode instabilities to be present also in YHG models. A corresponding study will be presented elsewhere.

ACKNOWLEDGEMENTS

MK acknowledges financial support from the Czech Science Foundation (GA ČR 20-00150S). The Astronomical Institute Ondřejov is supported by RVO:67985815. This work is part of the project ‘Support of the international collaboration in astronomy (ASU mobility)’ with the number CZ.02.2.69/0.0/0.0/18_053/0016972. ASU mobility is co-financed by the European Union. This project has also received funding from the European Union’s Framework Programme for Research and Innovation Horizon 2020 (2014–2020) under the Marie Skłodowska-Curie Actions Grant Agreement No. 823734. We acknowledge support by the Open Access Publication Funds of the Göttingen University.

DATA AVAILABILITY

The data underlying this article will be shared on reasonable request to the corresponding author.

REFERENCES

- Aret A., Kolka I., Kraus M., Maravelias G., 2017, in Miroshnichenko A., Zharikov S., Korčáková D., Wolf M., eds, ASP Conf. Ser. Vol. 508, The B[e] Phenomenon: Forty Years of Studies. Astron. Soc. Pac., San Francisco, p. 239
- Baker N., Kippenhahn R., 1962, *Z. Astrophys.*, 54, 114
- Baker N., Kippenhahn R., 1965, *ApJ*, 142, 868
- Böhm-Vitense E., 1958, *Z. Astrophys.*, 46, 108
- Cox J. P., 1980, *Theory of Stellar Pulsation*. Princeton Univ. Press, Princeton, NJ
- Davies B., Figer D. F., Law C. J., Kudritzki R.-P., Najarro F., Herrero A., MacKenty J. W., 2008, *ApJ*, 676, 1016
- de Jager C., 1998, *A&AR*, 8, 145
- de Jager C., Nieuwenhuijzen H., 1997, *MNRAS*, 290, L50
- de Jager C., Lobel A., Nieuwenhuijzen H., Stothers R., 2001, *MNRAS*, 327, 452
- Ekström S. et al., 2012, *A&A*, 537, A146
- Gautschy A., Glatzel W., 1990a, *MNRAS*, 245, 154
- Gautschy A., Glatzel W., 1990b, *MNRAS*, 245, 597
- Glatzel W., 1994, *MNRAS*, 271, 66
- Glatzel W., 2009, *Commun. Asteroseismol.*, 158, 252
- Glatzel W., 2021, in Kraus M., Torres A. F., eds, *Proceedings of the VIII La Plata International School ‘Pulsations Along Stellar Evolution’*, Vol. 12, Workshop Series of the Asociacion Argentina de Astronomia, La Plata, Argentina . p.73
- Glatzel W., Gautschy A., 1992, *MNRAS*, 256, 209
- Glatzel W., Kaltschmidt H. O., 2002, *MNRAS*, 337, 743
- Glatzel W., Kiriakidis M., 1993, *MNRAS*, 263, 375

- Glatzel W., Kiriakidis M., 1998, *MNRAS*, 295, 251
- Glatzel W., Mehren S., 1996, *MNRAS*, 282, 1470
- Glatzel W., Kiriakidis M., Chernigovskij S., Fricke K. J., 1999, *MNRAS*, 303, 116
- Gordon M. S., Humphreys R. M., 2019, *Galaxies*, 7, 92
- Gorlova N., Lobel A., Burgasser A. J., Rieke G. H., Ilyin I., Stauffer J. R., 2006, *ApJ*, 651, 1130
- Grott M., Chernigovskij S., Glatzel W., 2005, *MNRAS*, 360, 1532
- Hrivnak B. J., Kwok S., Geballe T. R., 1994, *ApJ*, 420, 783
- Humphreys R. M., 1978, *ApJS*, 38, 309
- Humphreys R. M. et al., 2006, *AJ*, 131, 2105
- Iglesias C. A., Rogers F. J., 1996, *ApJ*, 464, 943
- Jura M., Kleinmann S. G., 1990, *ApJ*, 351, 583
- Kiriakidis M., Fricke K. J., Glatzel W., 1993, *MNRAS*, 264, 50
- Klochkova V. G., 2019, *Astrophys. Bull.*, 74, 475
- Koumpia E. et al., 2020, *A&A*, 635, A183
- Kourniotis M., Kraus M., Maryeva O., Borges Fernandes M., Maravelias G., 2022, *MNRAS*, 511, 4360
- Kraus M., Kolka I., Aret A., Nickeler D. H., Maravelias G., Eenmäe T., Lobel A., Klochkova V. G., 2019, *MNRAS*, 483, 3792
- Kraus M., Liimets T., M. Arias L., Moiseev A., Cidale L. S., Torres A. F., Nickeler D. H., 2022a, *Azerbaijani Astron. J.*, 17, 7
- Kraus M., Arias M. L., Cidale L. S., Torres A. F., Kourniotis M., 2022b, *Bol. Asoc. Argentina Astron. La Plata Argentina*, 63, 65
- Kraus M., Kourniotis M., Arias M. L., Torres A. F., Nickeler D. H., 2023, *Galaxies*, 11, 76
- Lagadec E., Zijlstra A. A., Oudmaijer R. D., Verhoelst T., Cox N. L. J., Szczerba R., Mékarnia D., van Winckel H., 2011, *A&A*, 534, L10
- Lambert D. L., Hinkle K. H., Hall D. N. B., 1981, *ApJ*, 248, 638
- Ledoux P., Walraven T., 1958, *Handbuch der Physik*, Vol. 51, Springer, Berlin, p.353
- Lobel A., 2001, *ApJ*, 558, 780
- Lobel A., de Jager C., Nieuwenhuijzen H., Smolinski J., Gesicki K., 1994, *A&A*, 291, 226
- Lobel A., Israelian G., de Jager C., Musaev F., Parker J. W., Mavrogiorgou A., 1998, *A&A*, 330, 659
- Lobel A. et al., 2003, *ApJ*, 583, 923
- McGregor P. J., Hillier D. J., Hyland A. R., 1988, *ApJ*, 334, 639
- Maravelias G., Kraus M., 2022, *J. Am. Assoc. Var. Star Obs.*, 50, 49
- Nieuwenhuijzen H., de Jager C., 1995, *A&A*, 302, 811
- Oksala M. E., Kraus M., Cidale L. S., Muratore M. F., Borges Fernandes M., 2013, *A&A*, 558, A17
- Oudmaijer R. D., de Wit W. J., 2013, *A&A*, 551, A69
- Oudmaijer R. D., Davies B., de Wit W. J., Patel M., 2009, in Luttermoser D. G., Smith B. J., Stencel R. E., eds, *ASP Conf. Ser. Vol. 412, The Biggest, Baddest, Coolest Stars*. Astron. Soc. Pac., San Francisco, p. 17
- Percy J. R., Kolin D. L., Henry G. W., 2000, *PASP*, 112, 363
- Rogers F. J., Iglesias C. A., 1992, *ApJS*, 79, 507
- Rogers F. J., Swenson F. J., Iglesias C. A., 1996, *ApJ*, 456, 902
- Saio H., 2011, *MNRAS*, 412, 1814
- Saio H., Georgy C., Meynet G., 2013, *MNRAS*, 433, 1246
- Shenoy D. et al., 2016, *AJ*, 151, 51
- Smartt S. J., 2009, *ARA&A*, 47, 63
- Stothers R. B., 1999, *MNRAS*, 305, 365
- Stothers R. B., Chin C.-W., 1993, *ApJ*, 408, L85
- Stothers R. B., Chin C.-W., 2001, *ApJ*, 560, 934
- Tiffany C., Humphreys R. M., Jones T. J., Davidson K., 2010, *AJ*, 140, 339
- Zsoldos E., Percy J. R., 1991, *A&A*, 246, 441

This paper has been typeset from a $\text{\TeX}/\text{\LaTeX}$ file prepared by the author.